<div align="center">

Supporting Material for

FCHo Proteins are Nucleators of Clathrin-Mediated Endocytosis

</div>

William Mike Henne[1],[2],[*], Emmanuel Boucrot[1],[*],[†], Michael Meinecke[1], Emma Evergren[1], Yvonne Vallis[1], Rohit Mittal[1] and Harvey T. McMahon[1],[†]

[1] MRC Laboratory of Molecular Biology, Hills Road, Cambridge, CB2 0QH, UK

[2] present address: Weill Institute for Cell and Molecular Biology, Cornell University, Ithaca, NY 14853, USA.

[*] These authors contributed equally to this work.

[†] To whom correspondence should be addressed: hmm@mrc-lmb.cam.ac.uk and eboucrot@mrc-lmb.cam.ac.uk

Materials and methods

      Plasmids, cloning and protein purification

      Antibodies

      Cryo-Immuno electron microscopy

      Cell culture, transfection, and RNAi

      Protein pull-down experiments

      Live-cell fluorescent microscopy and analysis

      Rat hippocampal neuron cultures and synaptic-vesicle endocytosis (SypHy)

      Immunostaining and ligand uptakes (transferrin, EGF and LDL)

      Liposome co-sedimentation and *in vitro* tubulation assays

Supporting text, technical considerations

      Overexpression of tagged FCHo proteins

      RNAi depletion

      FCHo proteins and synaptic vesicle recycling

      F-BAR-x lipid specificity and twisted tubules

Supporting discussion

Figures S1-12

Supplementary movie legends

Author contributions

Supporting references

Materials and methods:

Plasmids, cloning and protein purification. Full length mouse FCHo2 (Riken AK142282) and human FCHo1 (IMAGE 5757146) were cloned into pGEX6P1 and pEGFP (Clontech), pTagRFP, and pTagBFP vectors (Evrogen). We introduced a point mutation (S158T) rendering TagRFP more photostable (S1) into the pTagRFP plasmids used for all TagRFP constructs of this study. For simplicity EGFP, TagRFP and TagBFP are called 'GFP', 'RFP' and BFP' in the text and figures. Mammalian expression of untagged constructs of FCHo1 and FCHo2 used in the titration experiments (Fig. 1F-H and S5) were generated by cloning into pEGFP-N3 with a stop codon introduced by mutagenesis before the EGFP sequence and verified by sequencing. The F-BAR (1-262), F-BAR-x (1-327), extended region "x" (263-430), and μHD (525-809) of FCHo2 were cloned separately. The FCHo2 chimera was generated by inserting the middle region and μHD of FCHo2 (395-809) into a construct expressing EGFP-PLCδ PH domain (1-175) at its N-terminus, a kind gift of Matilda Katan (S2), plus a 17 amino acid linker region. The RNAi-resistant form of FCHo2 used in the 'rescue' experiments was generated by introducing the following mutations D310D (GAT-GAC), A311L (GCA-TTA) and L314L (CTT-TTG). Rat EGFP-LCa (Clathrin Light chain a) was a kind gift of Margaret Robinson (University of Cambridge, UK). RFP-LCa was generated by transfer of the LCa gene into pTagRFP. EGFP-intersectin(ITSN)1L was a kind gift from Peter McPherson (McGill University, Canada) (S3). RFP-ITSN, and BFP-ITSN were generated by transfer of the intersectin 1L gene into pTagRFP and pTagBFP vectors, respectively. Human eps15 (1-896) was cloned from a construct from Alexandre Benmerah (Institut Cochin, Paris) (S4, S5) and transferred into pEGFP, pTagRFP or pTagBFP vectors to generate GFP-eps15, RFP-eps15 and BFP-eps15, respectively. EGFP-rapostlinS (FBP17 short form) was a kind gift from Manabu Negishi (Kyoto University, Japan) (S6). SypHy (synaptophysin-fluorin) was a kind gift from Leon Lagnado (S7). For testing the direct binding of eps15 to FCHo2 μHD, a construct corresponding to the C-terminal region (residues 530-791) of human eps15 was cloned and purified by GSH-sepharose gel chromatography. Mouse Dab2/p96 (residues 1-548) was cloned from a construct originally from Shelli Morris (S8). Rat Epsin1-myc was cloned as previously described (S9). AP180 C-terminus (residues 530-915), described previously (S10), was transferred into pTagBFP. Point mutations were made by PCR mutagenesis and constructs were sequenced. GST-tagged constructs were expressed in BL21 *E.coli* (Stratagene) and purified on GSH-sepharose beads (GE Healthcare), tags were cleaved with PreScission protease (GE Healthcare), and proteins were subsequently purified by ion exchange and gel filtration chromatography.

Clathrin-coated vesicles (Fig. 2D) were enriched as in (S11).

Antibodies. For Western blotting and immunofluorescence (IF) studies, the following antibodies were used: anti-FCHo2 Ra103 (in house affinity purified rabbit polyclonal raised against residues 3-274 of human FCHo2 F-BAR domain), anti-eps15/eps15R Ra15 (in house rabbit polyclonal raised against human eps15 539-896), anti-actin 6276ab (Abcam mouse monoclonal), anti-Dab2/p96 D45720 (mouse monoclonal, Transduction Laboratories), anti-intersectin S750 (rabbit polyclonal, a kind gift from Tom Südhof), anti-AP2 α–adaptin for IF

staining 2730ab (mouse monoclonal, Abcam), anti-AP2 α–adaptin for Western blotting A43920 (mouse monoclonal, Transduction Laboratories), anti-synaptophysin P38/CL43.1 (mouse monoclonal, a kind gift from Reinhart Jahn), anti-clathrin heavy chain (CHC) for immunofluorescence studies X22 (mouse monoclonal, a kind gift from Frances Brodsky), anti-clathrin heavy chain for Western blotting 610500 (mouse monoclonal, Transduction Laboratories) and anti-GFP for cryoimmuno-electron microscopy ab290 (rabbit polyclonal, AbCam), anti-dynamin Hudy-1 (05-319) (mouse monoclonal, Upstate), anti-synaptotagmin1 V216 (rabbit polyclonal monoclonal, a kind gift from Tom Südhof) and anti-EGFR antibody 13A9 (mouse monoclonal, a kind gift from Genentech).

Cryo-immuno electron microscopy (Fig. 1B and 2E). HEK293T cells expressing EGFP-FCHo2 were fixed in 2% paraformaldehyde/0.2% glutaraldehyde in phosphate buffered saline (PBS). The cells were pelleted in 1% gelatine in PBS at 37°C, resuspended in 12% gelatine in PBS, pelleted and solidified on ice. Small blocks (~0.5 mm) of the cell pellet were prepared and infiltrated with 2.3 M sucrose at 4°C overnight, and then mounted on aluminium stubs, frozen and sectioned. The sections (60nm) were picked up in drops of 2.3M sucrose and collected on Formvar-coated, carbon-coated nickel mesh grids. After blocking in 0.1% BSA in PBS the sections were incubated with an anti-GFP antibody (0.25mg/ml; AbCam ab290), washed, and incubated with a secondary antibody conjugated to 15 nm gold particles (GE Healthcare). The sections were fixed in 1% glutaraldehyde and stained with ice cold 0.4% uranyl acetate/1.8% methyl cellulose (pH 4) and dried. The samples were viewed in a FEI Tecnai 12 transmission electron microscope. The density of gold particles in the upper and lower half (in an area of $0.02\mu m^2$) of 22 constricted clathrin-coated pits was quantified using ImageJ.

Cell culture, transfection, and RNAi. BSC1 cells (ECACC 85011422) and HeLa cells (ECACC 93021013) were cultured in DMEM-GlutaMAX-I media (Gibco) supplemented with 10% foetal bovine serum (FBS). Non-transformed hTERT-RPE1 cells (Clontech) were cultured in DMEM F12 HAM (Sigma) supplemented with 10% FBS, 2mM GlutaMAX-I (Gibco) and 0.25% sodium bicarbonate. BSC1 cells stably expressing σ2-EGFP (S12) were a kind gift of Tom Kirchhausen (Harvard Medical School, USA). For live-cell imaging (see details below), approximately $2x10^5$ cells were cultured on 35mm glass bottom dishes (MatTek). Cells were transfected using Lipofectamine 2000 (Invitrogen), using 0.1-1μg of the various plasmids (except for the titrations (Fig. 1F-H and fig. S5) where 0.5, 1 or 2μg of plasmids were used). Cells were typically incubated 24 hours to express the constructs before imaging. For gene silencing experiments, siRNAs were purchased from Invitrogen (Stealth Select siRNAs) or Dharmacon (ON-TARGETplus SMARTpool). RNAi oligos used were (all human): FCHo2 (HSS151016), FCHo1 (HSS118255), SGIP1 (HSS130804), AP2-μ subunit (HSS101955), Dab2 (HSS102610), intersectin1 (HSS109703), intersectin2 (HSS121345), eps15 (HSS103327), eps15R (J-004006-05), clathrin heavy chain (CHC, HSS174637), control siRNAs (WILDE000533). RNAi oligos were resuspended to a 20μM stock concentration, and delivered using Oligofectamine (Invitrogen) to a total final concentration of 80pM. Cells typically received two doses of siRNA with a one day interval and were used up to three days later. A final concentration of 160pM was used when only one transfection was performed. Most cell cultures did not display complete loss of

3

the RNAi-targeted protein, and this is likely due to the spectrum of knockdown degrees among cells in the same culture, as well as the relatively low transfection efficiency seen for the BSC1 cell line. However, the cells selected for imaging were assessed individually (Tf uptake or co-transfection marker, see 'RNAi depletion' paragraph above). For the GST-μHD pull-down experiments in μ2-depleted HeLa lysate, cells received μ2 RNAi treatment and were FACS sorted to enrich only cells eliciting μ2 knockdown. Briefly, RNAi-treated HeLa cells were exposed to 5mg/mL Alexa488-transferrin (A488-Tf) for 5 min at 37°C, quickly acid washed (pH 5.5, 4°C, to remove the surface-bound A488-Tf), and FACS sorted at 4°C. Only Tf^{neg} cells (~ 90%) were collected and used for GST-μHD pull-down experiments. A small fraction was lyzed and blotted for AP2 α-adaptin to confirm knockdown (fig. S7B).

Protein pull-down experiments. (Fig. 2A, F and J). To test for interactions between proteins, GST-FCHo2 μHD (525-809) was produced in BL21 *E. coli* and purified as described above. GST-protein was eluted off of GSH-sepharose beads, further purified by gel filtration, and rebound to fresh GSH-sepharose beads for use in pull downs. HeLa cell or brain lysates (5-10mg/mL) were prepared in 150mM NaCl buffered with 20mM HEPES and 5mM DTT with added 0.1% Triton X-100 and a protease inhibitor cocktail (lysis buffer). Bead bound protein was then exposed to cell or rat brain lysate for 30 minutes to 1 hour, pelleted in a cooled desktop centrifuge, and washed three times in lysis buffer. The final pellet was boiled in sample buffer and ran on SDS-PAGE. For protein identification, Coomassie Brilliant Blue-stained protein bands were excised from the gels and underwent LC-MS-MS mass spectrometry for identification.

Live-cell fluorescent microscopy and analysis. Cells were grown on MatTek dishes and before imaging the medium was changed to α-MEM without phenol red supplemented with 20 mM HEPES, pH 7.4 and 5 % FBS and placed into a temperature controlled chamber on the microscope stage with 95% air:5% CO_2 and 100 % humidity. Live-cell imaging data were acquired using a fully motorized inverted microscope (Eclipse TE-2000, Nikon) equipped with a CSU-X1 spinning disk confocal head (UltraVIEW VoX, Perkin-Elmer, England) using a 60x lens (Plan Apochromat VC, 1.4 NA, Nikon) under control of Volocity 5.0 (Improvision, England). 14-bit digital images were obtained with a cooled EMCCD camera (9100-02, Hamamatsu, Japan). Four 50 mW solid-state lasers (405, 488, 561 and 647 nm; Crystal Laser and Melles Griots) coupled to individual acoustic-optical tunable filter (AOTF) were used as light source to excite TagBFP, EGFP, Alexa488, TagRFP, Alexa546 and Alexa647, as appropriate. Rapid two- or three-colours time-lapses were acquired at 500ms to 1s intervals, using a dual (525/50; 640/120, Chroma) and a triple filter (450/25; 525/40; 600/35, Chroma), respectively. The power of the lasers supported excitation times of 50ms in each wavelength and the AOTFs allowed minimum delay between 2 colours (e.g. delay between green-red for each timepoint), which was an important factor during the measurement of the timing of incorporation of the various CCP components we investigated.

Automated unbiased identification of all clathrin or AP2 fluorescent spots and quantitative tracking of their dynamics as a function of time were performed using SlideBook 4.1 (Intelligent Imaging Innovations) following the same criteria and procedures as in (S12, S13).

The graph on Fig. 1A represents 10 representative pits of equal length (60s). The fluorescence intensities (a.u.: arbitrary units), corrected for their respective surrounding background, of RFP-FCHo2 and GFP-LCa were plotted versus time. Zero '0' values correspond to background levels (for y-axis, intensities) and to the timeframe before RFP-FCHo2 intensity became above background levels (for x-axis, time), respectively. Nucleation rates (Fig. 1D and G, fig. S5) represent the number of new CCPs / 10^4 μm^2 / second. Statistical significances (p values) were calculated by unpaired two-tailed Student's t-test. p values inferior to 0.01 were considered significant. Colocalization scorings (fig. S1E, F and S2E) were performed on at least 500 dynamic CCPs (kymographs), from 3 cells imaged during independent experiments. The scorings annotated on each kymograph represent the proportion of CCPs profiles that displayed the phenotype shown in the representative kymographs reported (to report that the kymographs displayed are truly representative). For exemple, in Fig. 1A, 91±5% (mean ± standard deviation (SD)) of 319 CCPs (from 3 cells imaged during independent experiments) had detectable RFP-FCHo2 at least 2 timeframes before GFP-CLC. Apart for fig. S2E where the number of CCPs which had detectable FBP17 was very low (~3%) and only 50 CCPs could be analysed, all the other scorings were done on at least 200 (up to 400 in some cases) CCPs analysed randomly, from 3 cells imaged during independent experiments.

For experiments (fig. S10D) involving the addition of tert-butanol or 1-butanol to culture media (S13), a 4% alcohol stock buffer (in DMEM) was added in equal volume directly into the cell culture dish to give a final concentration of 2% tert- or 1-butanol. Washout was performed by decanting the total media in the culture dish and quickly replacing with fresh media. Cells were imaged continually throughout the process.

Rat hippocampal neuron cultures and synaptic-vesicle endocytosis (SypHy). E18 day old pups were harvested from Sprague-Dawley rats in accordance with UK Animal policy. The hippocampus was excised and placed into ice-cold EBSS buffer (Gibco) supplemented with 10mM HEPES and Penicillin/Strep mix. Hippocampi were placed into warm buffer with added papain protease (10U/mL), mechanically homogenized into 2mLs of culture medium, and decanted onto 16mm MatTek glass-coverslip dishes coated with poly-D-lysine (50μg/mL) and laminin (20μg/mL). Cultures were typically analysed at 4 DIV (days in vitro). Cultured neurons were transfected via electroporation in an Amaxa Nucleofector machine according to the manufacturer's protocol. Alternatively, cultured neurons were transfected with lipofectmine 2000 at 7 DIV and analysed at 15 DIV according to (S7). SypHy experiments were performed in a pH 7.4 extracellular medium containing 10mM glucose, 136mM NaCl, 2.5mM KCl, 10mM HEPES, 1.3mM $MgCl_2$, 2mM $CaCl_2$, 0.01mM CNQX and 0.05mM DL-APV, according to (S7). Neurons were imaged at 1Hz using spinning-disk confocal microscopy system described above. Neurons depolarization was achieved by application of extracellular medium containing 50mM KCl for 30 sec, followed by a washout into the pH 7.4 extracellular medium. Quenching (pH5.5 medium) was perform at the end of recording to confirm the SypHy signal was at the at the neurons surface.

Immunostaining and ligand uptakes (transferrin, EGF and LDL). For immunofluorescence staining (fig. S1C), cells were grown on glass coverslips, fixed with 3.7% paraformaldehyde and

permeabilized with either 0.1% saponin or 0.1% Triton X-100 for 1 hour room temperature in 10% goat serum. Primary and secondary antibodies were delivered in 1% goat serum, and cells were washed in PBS before being mounted with DABCO anti-fade agent on glass slides. For surface staining of synaptotagmin1 (Syt1, fig. S4D), neurons were incubated at 4°C for 1h with the V216 antibody (rabbit) in 10% goat serum in PBS without prior permeabilization of the neurons. After wash of the unbound antibody, the neurons were fixed with 3.7% paraformaldehyde, and the antibody revealed with anti-rabbit-conjugated secondary antibody. To measure transferrin, EGF and LDL uptake, cells grown on coverslips were incubated with either 10μg/mL Alexa546-transferrin, 50μg/mL anti-EGFR monoclonal antibody (13A9) together with 2ng/mL unlabelled-EGF (a concentration of EGF ligand that activate principally clathrin-mediated endocytosis (S14)) or 1μg/mL Dil-LDL for 5minutes at 37°C. Cells were washed with ice-cold PBS to halt uptake and remove unbound ligands. Cells were then briefly acid washed (3 washed, 2 min with pH 5.5 buffer, at 4°C) to remove surface-bound ligands, fixed in 3.7% paraformaldehyde and mounted on slides. Imaging of fixed-samples (endogenous staining and transferrin, EGF and LDL uptake) was performed with the same confocal imaging system described above. Three-dimensional (3D) stacks were acquired with a piezo-driven stage using 0.3 μm steps. All the Tf, EGF and LDL signals contained within the boundaries (PM) of each cells (measured on 3D stacks of images) were quantified and background-corrected. The values were normalized to the mean (average) of the control set to 100. The quantification represents the mean ± standard deviation (SD) of at least 50 cells in each category, from 3 independent experiments. Statistical significances (p values) were calculated by unpaired two-tailed Student's t-test. p values inferior to 0.01 were considered significant.

Liposome co-sedimentation and in vitro tubulation assays. (Fig. 3B and C, fig. S10B, C and S11C). For protein-membrane binding experiments, liposomes were made by pore extrusion. Liposomes were composed of 80% Folch brain derived lipids (Avanti Polar Lipids, item 131101P) 15% phosphatidylserine (PS), and 5% Pi(4,5)P2 . Lipid components were mixed in 1:1 chloroform:methanol, dried in glass tubes by Argon gas, rehydrated into buffer (150mM NaCl, 20mM HEPES pH 7.4, and 2.5mM DTT), sonicated at 37°C, and filtered through Whatman 0.8μm diameter polycarbonate filters to a final concentration of 1mg/ml. For lipid co-sedimentation assays, 15μM protein was incubated with 0.5mg/ml liposomes for 30 minutes at room temperature, and then spun down in a benchtop ultracentrifuge (Optima TL Ultracentrifuge) for 10 minutes at 70,000rpm (rotor TLA100). The supernatant was separated from the pellet, both were resuspended in sample buffer, and samples were boiled and run on SDS-PAGE gels. For in vitro tubulation assays, protein was incubated with 0.5mg/ml liposomes in 1.5ml eppendorf tubes at room temperature for 15-30 minutes and pipetted onto glow discharged carbon-coated copper TEM grids (Agar brand) for ~1 min. Grids were negative stained with 2% uranyl acetate for 60 seconds, washed in water briefly, and dried by blotting. Samples were examined on a PW6010/20 EM2055 transmission electron microscope (Phillips).

Supporting text, technical considerations:

Overexpression of fluorescently-tagged versions of FCHo1/2 proteins. We observed that, even at low expression levels, C-terminally tagged versions of FCHo1/2 (e.g. FCHo2-EGFP) had a severe dominant-negative effect on CCPs dynamics (which were very slow) and Tf uptake (impaired) (not shown). This was consistent with the reported inhibition of Tf and LDL uptake in cells overexpressing FCHo1-EGFP (S15) and slowed dynamics of CCPs reported under SGIP1α-GFP (S16). This effect is likely due to a compromised effectiveness of the μHD – however this is speculation, as we did not test the effectiveness of this fusion protein to bind to eps15 or intersectin.

In this study, we used N-terminally tagged versions of FCHo1/2 and SGIP1 (e.g. EGFP-FCHo2) since they did not perturb CCP dynamics and Tf uptake, as long as they were used <u>at very low levels of overexpression</u> and observed after a short time of overexpression (12 to 20 hours). We typically transfected 0.1-0.2 μg of DNA (without scaling down the lipofectant) per 10 cm^2 dishes containing ~2x10^5 cells. This led to ~15-30 % cells displaying very low levels of overexpression. The movies generated with N-terminally tagged versions of FCHo1/2 and SGIP1 were individually assessed for their CCP dynamics before being further used. These criteria were considered to be legitimate since overexpression of untagged versions of FCHo1 and FCHo2 - even with 2 μg of plasmid per 10 cm^2 dishes containing ~2x10^5 cells – dramatically increased the number of CCPs and Tf uptake (see Fig. 1F-H and S5).

RNAi depletion. For RNAi experiments we confirmed knockdown of the said protein by immunoblotting on the complete cell population treated with RNAi (Fig. S8A, B, C, and G). This analysis underestimates the efficiency of knockdown in an individual cell as there is generally a low transfection efficiency (~20%) as judged by the expression of RFP-tagged respective protein. To correct for this (Fig. S8D) we have quantified the protein expression levels compared with controls (no RNAi) and normalized these for the numbers of cells (using actin as an internal control in each sample). Then we corrected for the 20% transfection efficiency thus giving a more accurate view of how much the said protein was depleted in the cells imaged by live-cell imaging.

FCHo proteins and synaptic vesicle recycling. FCHo proteins nucleate clathrin in 4 DIV (days in vitro) hippocampal neurons and are required for normal synaptic vesicle markers recycling. Given the expression of FCHo1/2 in the brain, we depleted FCHo proteins in 4 DIV cultured hippocampal neurons and found that clathrin puncta on neurites were decreased (fig. S4B-C). Inhibition of clathrin-mediated endocytosis induces surface accumulation of synaptic vesicle markers, like synaptotagmin-1, which fail to recycle following exocytosis (S17). Upon FCHo1+2 RNAi, we observed a concomitant accumulation of the endogenous synaptotagmin-1 on the plasma membrane as detected by a monoclonal antibody against a luminal epitope of synaptotagmin that will be exposed on vesicle collapse (fig. S4D). To follow the kinetics of synaptic vesicle marker endocytosis, we used the SypHy reporter (pH-sensitive pHluorin fused to an intracellular loop of the synaptic vesicle protein, synaptophysin), which has been shown to be internalized by clathrin-mediated endocytosis (S7). After depolarization, increased SypHy

signals (the result of synaptic vesicles exocytosis) progressively decreased back to resting levels in control cells but remained elevated for longer in FCHo1+2 RNAi treated neurons, as a consequence of a reduction in endocytosis (fig. S4E). We concluded that FCHo1/2 proteins are nucleators of clathrin-mediated endocytosis in 4 DIV hippocampal neurons and are required for normal synaptic vesicle markers recycling.

F-BAR-x lipid specificity and twisted tubules. The FCHo2 F-BAR-x module bound preferentially to $Pi(4,5)P_2$-containing liposomes. As with all BAR-membrane interactions the interaction was concentration dependent, but we also note that the preference for $Pi(4,5)P_2$ was not as evident at high protein concentrations ($20\mu M$ +), where binding to $Pi(3,5)P_2$-liposomes but not $Pi(3)P$-liposomes could now be observed. Where we see significant membrane binding then we can also detect tubulation, suggesting that significant binding naturally leads to membrane deformation. It is evident in Fig. 3C that the narrow 18nm tubules are twisted. It is likely that the protein induces this twisting as the membrane interaction sites are not precisely along the concave face of the F-BAR structure. On the extremities of the structure the membrane binding regions are positioned more towards the sides, and as the F-BAR module is symmetrical this results in the membrane twisting around the dimer module (unpublished observations).

Supporting discussion:

Altogether, this study places FCHo1/2 as part of a lipid-binding module that, by recruiting eps15 and intersectin, functions as a nucleator of clathrin vesicle budding. This study elucidates the centrality of membrane sculpting in the initiation of clathrin-mediated endocytosis and leads to a model (fig. S12) whereby AP2 is not the initiator of vesicle formation but is mainly an adaptor for clathrin, cargos and accessory proteins. The F-BAR domain found in FCHo2 can support a number of different curvatures from relatively flat to more extreme curvatures. Vesicle formation requires the generation of progressively higher curvatures. Given that this transition is observed for FCHo2 in vitro as increased protein concentrations leads to more extreme curvatures, we would propose that the narrow curvatures are likely facilitating vesicle neck formation and potentially provide a template for dynamin recruitment. Indeed we see FCHo2 at the rim of constricted CCP profiles by IEM (Fig. 2E). This notion is consistent with the recruitment of dynamin at CCPs toward the time when FCHo2 has passed its maximal signal (Fig. 1A and fig. S6D) and also the concomitance between the curvature produced by FCHo2 (below 20 nm diameter) and the diameter found to be optimal for dynamin spontaneous recruitment (S18). We also found that FCHo2 was not present in mature CCVs and we observed that the protein intensity frequently decreased before CCV budding, and if the protein intensity remained then there were multiple rounds of clathrin cycling. It is interesting that FCHo1/2 proteins did not bind directly to either AP2 or clathrin and thus this may ensure some time-lag between the initiation of curvature and vesicle maturation. All these observations are consistent with FCHo1/2 initiating curvature while being excluded from the final vesicle. FCHo2 binds to $Pi(4,5)P_2$ and thus provides some specificity for plasma membrane vesicle budding. Given the abundance of polylysine motifs in the F-BAR-x it could potentially help to

concentrate Pi(4,5)P$_2$, a key binding substrate for AP2, epsin, AP180/CALM, all components involved in CCP maturation (S9, S10, S19).

FCHo1/2 proteins also have a μHD that can be found in a number of other proteins and has recently been crystallized from the yeast Syp1p (S15). We show that binding of eps15 and intersectin to this domain is necessary for maturation of the coated-pit. This is likely because these proteins provide the link to AP2 (as each has an AP2 interaction region) and also eps15 is (at least) a dimer and may help crosslink the FCHo2 proteins, helping to concentrate them. Consistent with this, we observe that FCHo2 (while plasma membrane localized) is not clustered in the absence of eps15/eps15R and intersectins. It is notable that yeast Syp1p interacts with the yeast homologue of eps15 (Ede1) (S15). It points to a primordial origin for the clathrin pathway where sculpting and crosslinking proteins, rather than clathrin and its adaptors, may be the commonality between yeast and metazoans.

It is notable that the F-BAR-x (membrane binding/sculpting) and μHD (eps15/intersectin recruiting) domains function synergistically in FCHo1/2 to nucleate CCPs. Indeed, SGIP1 which contains a μHD that binds eps15 (S20) but lacks the F-BAR-x did not rescue CCP formation in the absence of FCHo1/2 (Fig 3A). Consistently, SGIP1 is not recruited early to CCPs (fig. S10A).

FCHo1/2 proteins are conserved across species and are ubiquitous in mammals and are thus likely to play a fundamental role in most CCV budding events from the plasma membrane, including synaptic vesicle endocytosis. These observations put curvature generation as fundamental to clathrin-coated pit formation and vesicle budding and place FCHo1/2 as the key initial element for nutrient uptake, receptor regulation and synaptic vesicle retrieval.
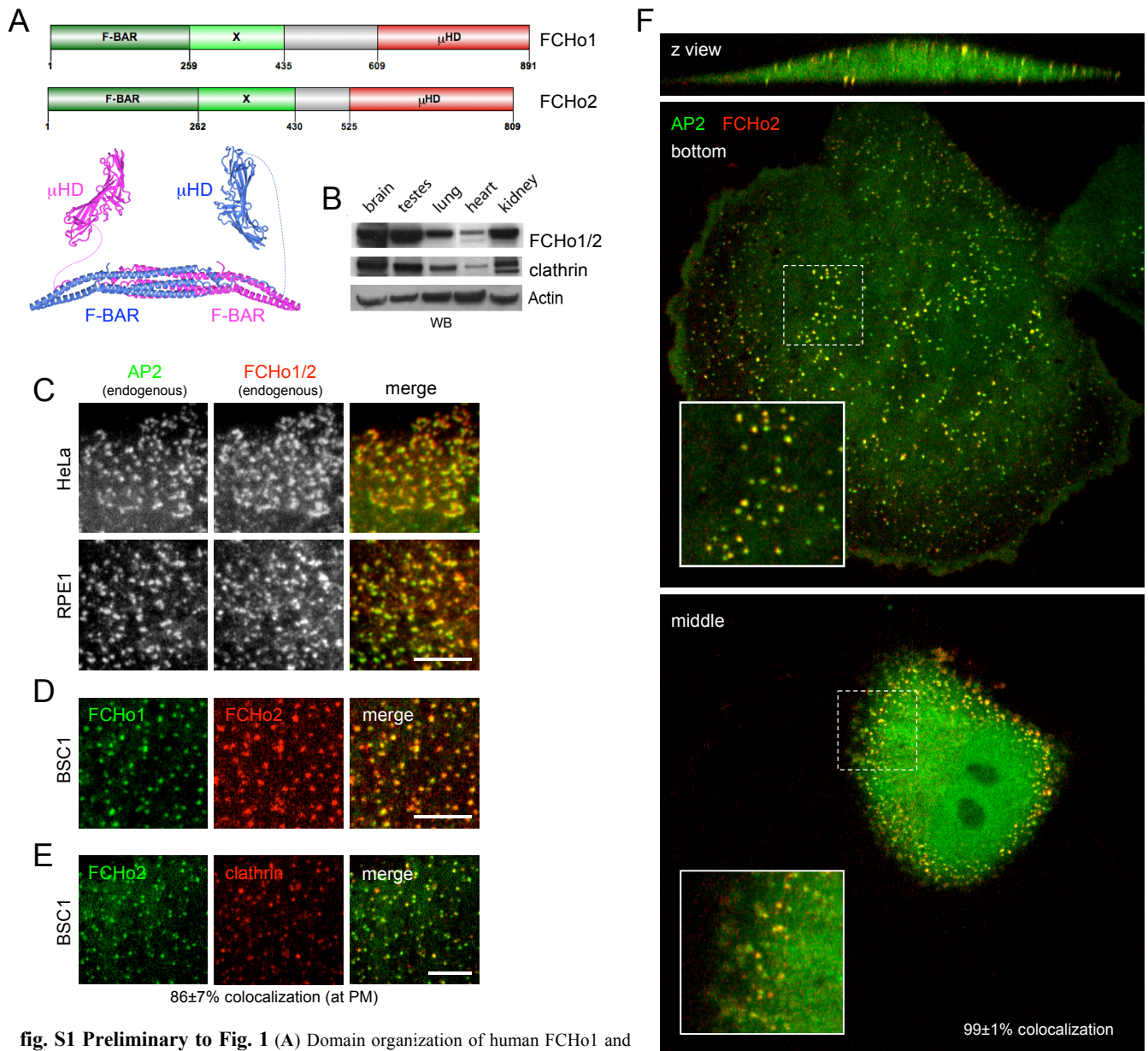
Supplementary figures

fig. S1 Preliminary to Fig. 1 (A) Domain organization of human FCHo1 and mouse FCHo2 (the clones used in this study). The proteins have a similar organization and contain N-terminal F-BAR domains (residues 1 to 262 in FCHo2), immediately followed by an extended (x) domain (residues 263-430) found in the yeast homolog Syp1p and in SGIP1 (S16) and which enhances lipid membrane binding (see fig. S10B). The region following the extended domain but prior to the μHD is predicted to be unstructured and shows very low sequence homology between FCHo proteins. In the yeast homolog Syp1p, this region has been shown to inhibit Las17/WASp-dependent actin assembly (S21). Both FCHo1 and FCHo2 end with C-terminal μHDs (a domain with homology with μ2-subunit of AP2 (see fig. S9A and (S15)) that are also found in stonin 1 and 2, δCOP, SGIP1 and the yeast homolog Syp1p (S15, S22). Bottom - FCHo2 F-BAR domains homodimerize. Syp1p μHD (S15) are shown at scale. **(B)** FCHo1/2 is expressed ubiquitously. The expression level of FCHo1/2 directly correlates with that of clathrin heavy chain (CHC). **(C)** Endogenous FCHo1/2 colocalize with endogenous AP2 (labelled with a monoclonal anti-α-adaptin) in human transformed HeLa and non-transformed RPE1 cells. **(D)** EGFP-FCHo1 (FCHo1) colocalizes with RFP-FCHo2 (FCHo2). **(E)** EGFP-FCHo2 (FCHo2) colocalizes with RFP-LCa (clathrin) on the plasma membrane of BSC1 cells. **(F)** RFP-FCHo2 colocalizes with σ2-EGFP (AP2), the plasma-membrane specific clathrin adaptor. Note that FCHo2 is detected mainly at the plasma membrane (z view, and insets). Scale bars, 5 (C-E) or 10 μm (F).
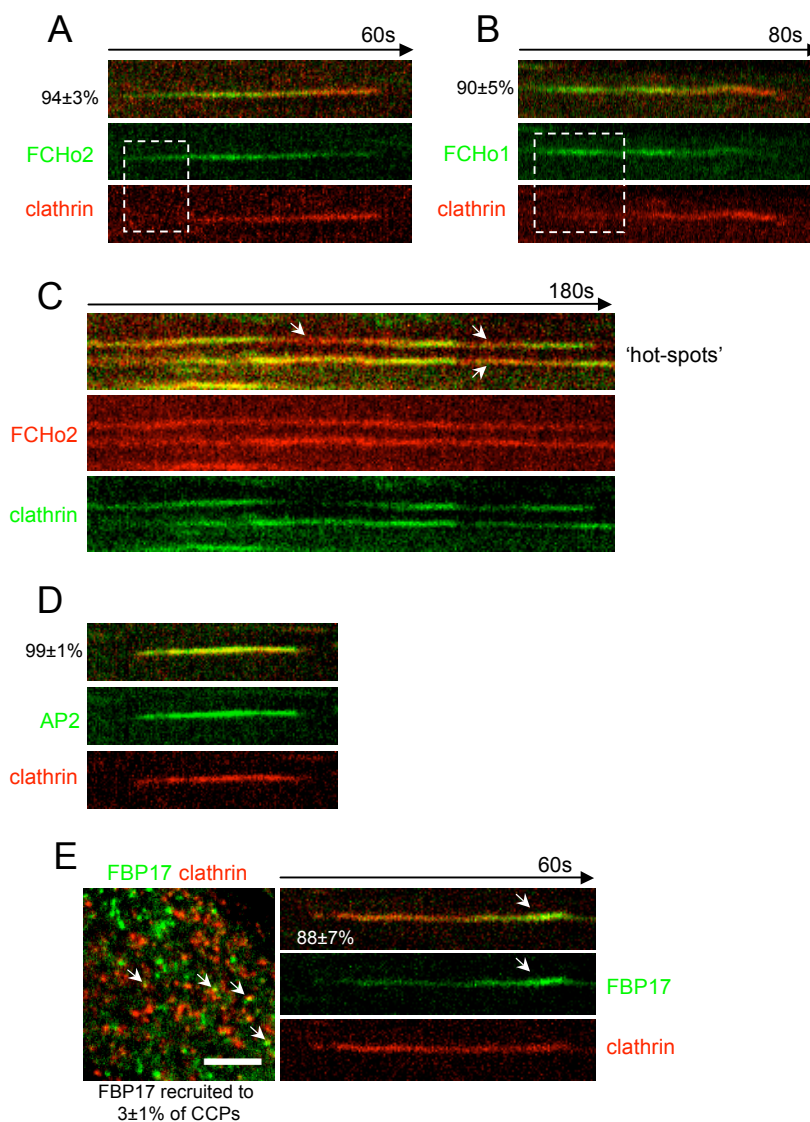
fig. S2 Supplement for Fig. 1A (**A**) Kymograph of a representative CCP labelled with GFP-FCHo2 (FCHo2) and RFP-LCa (clathrin) - inverse tags compared to Fig. 1A. Note the inversion of the tags did not affect the detection of FCHo2 before clathrin. (**B**) Kymograph of a representative CCP labelled with EGFP-FCHo1 (FCHo1) and RFP-LCa (clathrin). Like FCHo2, FCHo1 appeared prior to clathrin. (**C**) FCHo2 marked clathrin endocytic 'hot-spots'. Kymograph of RFP-FCHo2 and EGFP-LCa. FCHo2 and clathrin co-localized and when clathrin signal diminished, FCHo2 remained and marked a site where clathrin returns (arrows). (**D**) Kymograph of a representative CCP labelled with σ2-EGFP (AP2) and RFP-LCa (clathrin). AP2 was not detected before clathrin. (**E**) EGFP-FBP17 (FBP17) was recruited to 3±1% of CCPs (labelled with RFP-LCa (clathrin)) in BSC1 cells. Some colocalizations were nevertheless observed (arrows). Kymograph of a CCP labelled with EGFP-FBP17 and RFP-LCa. Note that FBP17 accumulated late (arrow) during CCP formation. Scale bars, 5 μm. Displayed kymographs were representative (percentage).
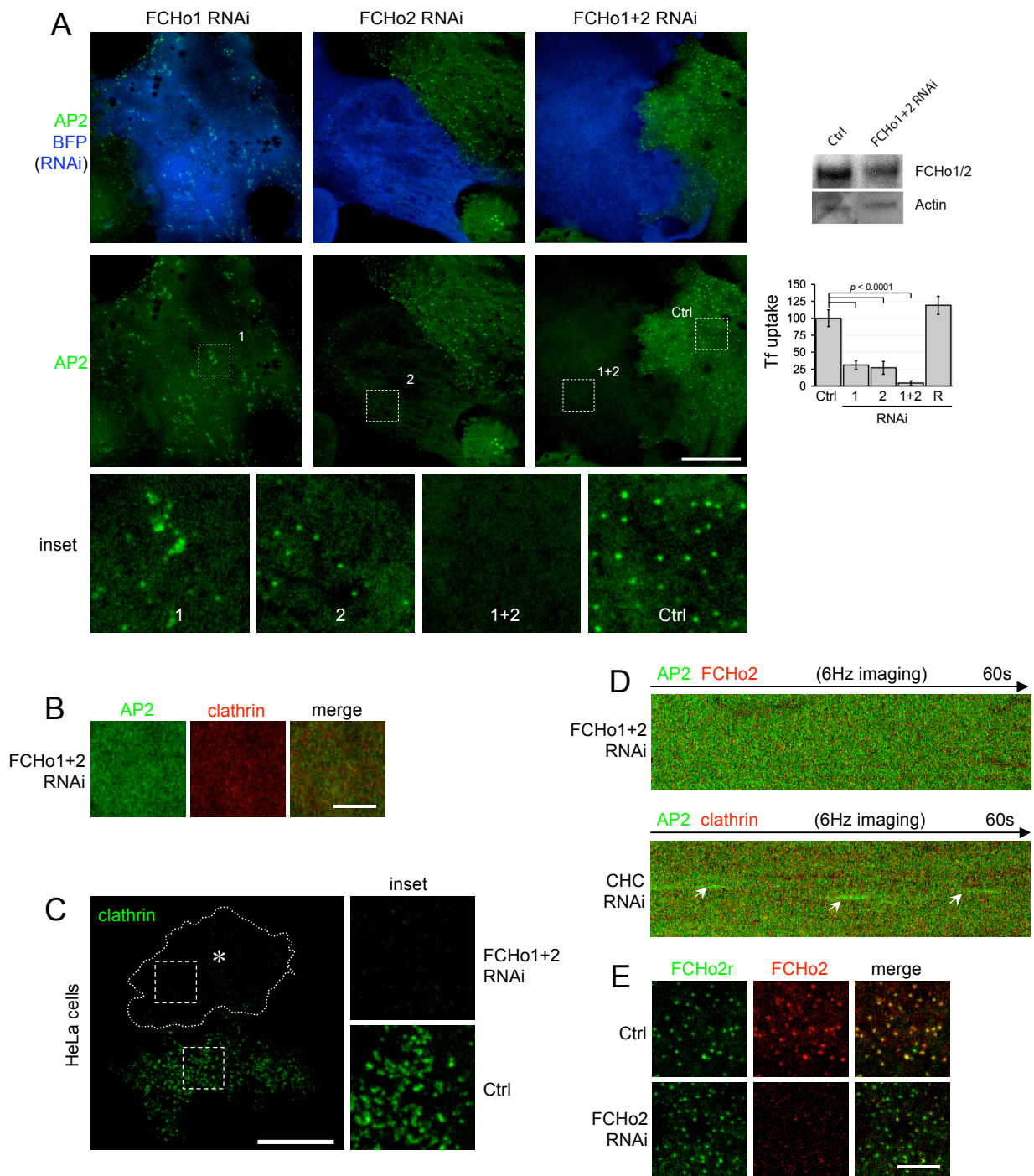
fig. S3 Supplement for Fig 1C (**A**) FCHo1+2 double RNAi was required for complete block of CCP nucleation and transferrin (Tf) uptake. BSC1 σ2-EGFP (AP2) cells co-transfected with BFP (transfection marker) and either Ctrl, FCHo1, FCHo2 or FCHo1+2 RNAi were mixed with non-transfected BSC1 σ2-EGFP cells and imaged live by spinning-disk confocal microscopy. Note the decrease of AP2 spots and Tf uptake (graph) in both FCHo1 and FCHo2 single-RNAi and the virtually total disappearance of AP2 spots and strong decreased of Tf uptake (graph) in FCHo1+2 double RNAi. (**B**) FCHo1+2 double RNAi stops nucleation of both σ2-EGFP (AP2) and RFP-LCa (clathrin), and their fluorescent signals are re-distributed to the cytoplasm (diffuse signals at the bottom confocal plane - contrast enhanced to insure that no puncta remained). (**C**) HeLa were transfected with FCHo1+2 RNAi for 2 days were mixed and plated with control cells for 24h, fixed and stained for endogenous clathrin. FCHo1+2 -depleted cells ('*', borders outlined) had reduced clathrin staining. Note that the first bottom confocal plane is displayed, normal clathrin signal was visible at the prinuclear region of both cells (**D**) High speed (6 Hz, or 1 frame every 166 ms) live-cell imaging could not detect AP2 nucleation in FCHo1+2 RNAi cells (contrast enhanced to insure that no puncta remained). By contrast, in clathrin heavy chain (CHC) RNAi cells, many transient (~1-6 sec) and weak recruitment events of AP2 (arrows) were observed. (**E**) RNAi resistant form of EGFP-FCHo2 (FCHo2r) colocalized with RFP-FCHo2 in control cells (Ctrl) and remained on the PM as puncta under FCHo2 RNAi conditions. RFP-FCHo2, however, became cytosolic and displayed decreased fluorescence indicative of being reduced by RNAi. Scale bars, 20 (A, C) and 10 μm (B, D).
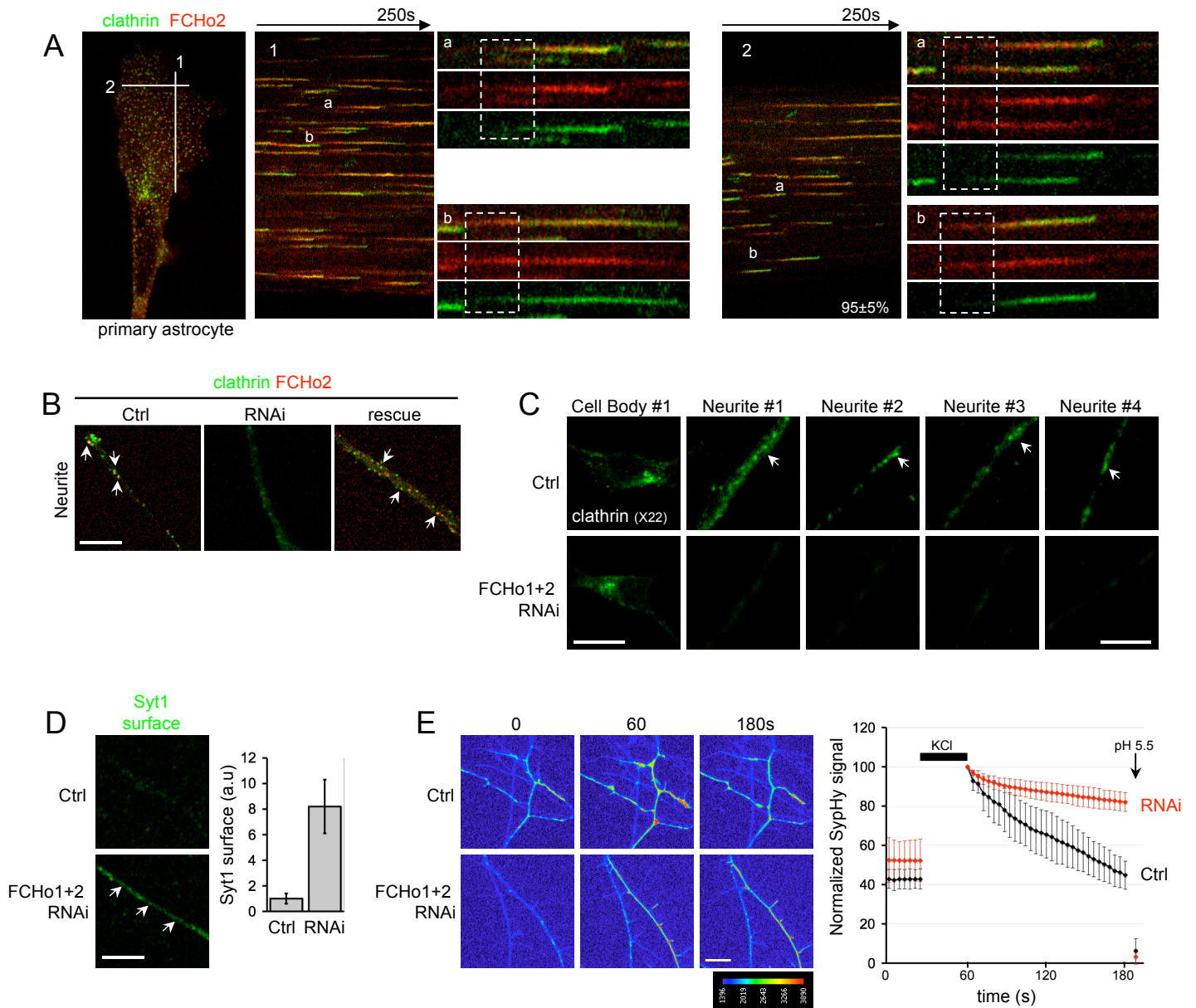
fig. S4 Supplement for Fig 1C (**A**) 4 DIV (days in vitro) rat primary astrocytes transfected with FCHo1+2 double RNAi and expressing EGFP-LCa (clathrin) and an RNAi-resistant form of RFP-FCHo2 (FCHo2). Kymographs 1 and 2 were generated along the respective lines. Note the detection of FCHo2 before clathrin (inset kymographs). Displayed kymographs were representative (percentage). (**B**) 4 DIV rat hippocampal neurons expressing EGFP-LCa (clathrin) and RFP-FCHo2 (FCHo2) displayed characteristic punctate staining along the neuronal processes (Ctrl, arrows), which were absent upon double RNAi of FCHo1+2 (RNAi). This inhibition was relieved by the co-expression of an RNAi-resistant form of RFP-FCHo2 (rescue). (**C**) 4 DIV hippocampal primary neurons transfected with FCHo1+2 double RNAi or not (Ctrl), fixed and stained for endogenous clathrin (X22 monoclonal antibody). Neurites from 4 different neurons in both categories are shown. Clathrin signals within neuronal cell bodies (endosomes, pericentriolar area) remained in FCHo1+2 RNAi neurons, but not the puncta on neurites (arrows). Scale bars, 10 and 5 μm for cell body or neurite pictures, respectively. (**D**) Surface staining of endogenous synaptotagmin 1 (Syt1) was low in the control (Ctrl, 1±0.4 a.u.) since Syt1 is recycled (S17) and increased under FCHo1+2 RNAi (8.2±2.1 a.u., normalized to the Ctrl (mean of Ctrl set to 1), indicating a decrease of clathrin-mediated endocytosis and synaptic vesicle recycling. (**E**) 4 DIV hippocampal neurons expressing SypHy (S7) and treated or not with FCHo1+2 RNAi were imaged at 1Hz by spinning-disk confocal microscopy. 50mM KCl were applied to depolarize the neurons and induce exocytosis. Intensity-coded colours are shown. Signals along neuronal projections form 3 neurons in each categories were quantified every 4s and normalized to 100 corresponding to the signals at the time of KCl washout. Neurons treated with FCHo1+2 had strongly decreased kinetics of SypHy endocytosis. Scale bars, 10 μm, unless specified.
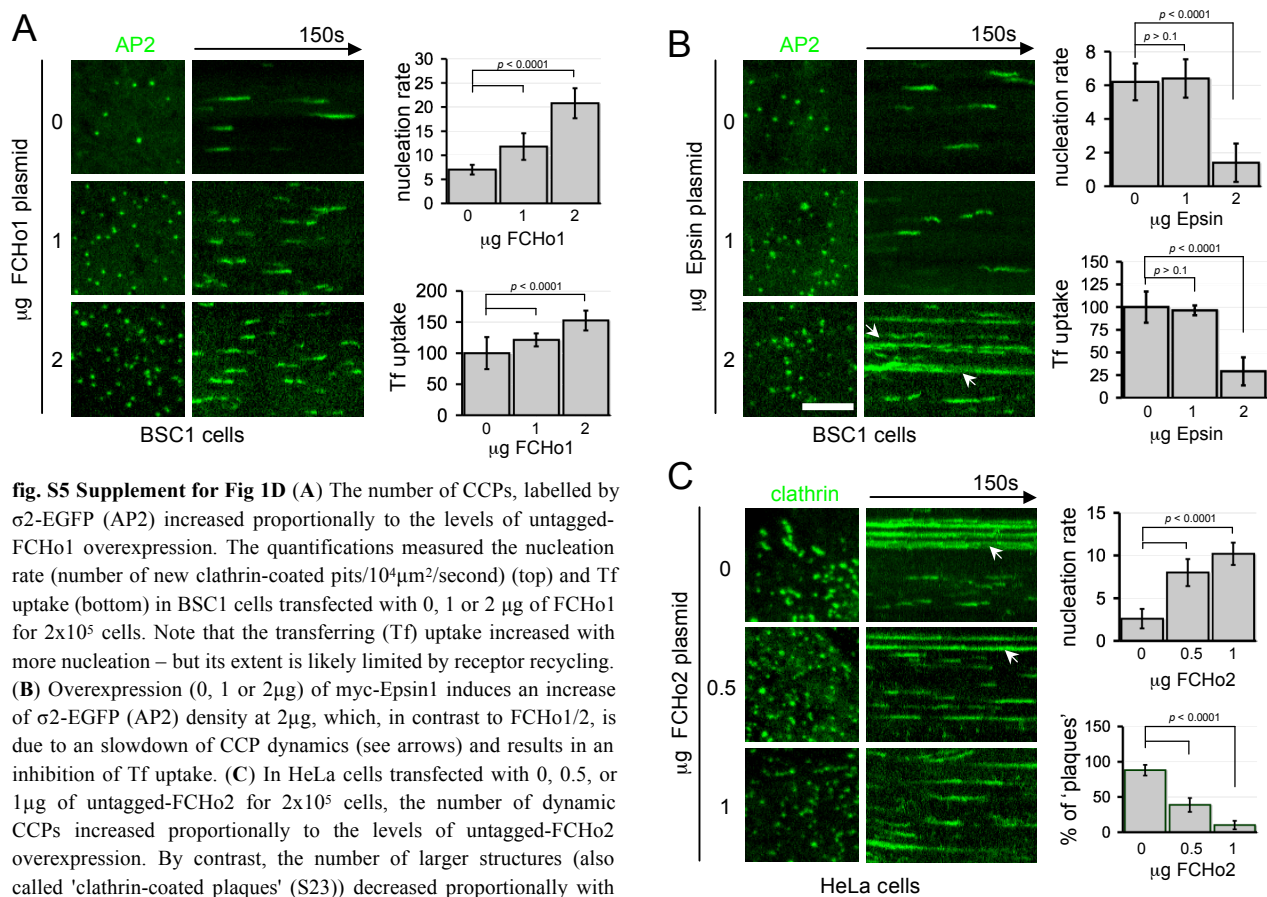
A AP2 150s

µg FCHo1 plasmid

0

1

2

BSC1 cells

nucleation rate
30
25
20
15
10
5
0
   0   1   2
   µg FCHo1
p < 0.0001

Tf uptake
200
150
100
50
0
   0   1   2
   µg FCHo1
p < 0.0001

B AP2 150s

µg Epsin plasmid

0

1

2

BSC1 cells

nucleation rate
8
6
4
2
0
   0   1   2
   µg Epsin
p > 0.1
p < 0.0001

Tf uptake
150
125
100
75
50
25
0
   0   1   2
   µg Epsin
p > 0.1
p < 0.0001

C clathrin 150s

µg FCHo2 plasmid

0

0.5

1

HeLa cells

nucleation rate
15
10
5
0
   0   0.5   1
   µg FCHo2
p < 0.0001

% of 'plaques'
150
100
50
0
   0   0.5   1
   µg FCHo2
p < 0.0001

fig. S5 Supplement for Fig 1D (**A**) The number of CCPs, labelled by
σ2-EGFP (AP2) increased proportionally to the levels of untagged-
FCHo1 overexpression. The quantifications measured the nucleation
rate (number of new clathrin-coated pits/10^4µm^2/second) (top) and Tf
uptake (bottom) in BSC1 cells transfected with 0, 1 or 2 µg of FCHo1
for 2×10^5 cells. Note that the transferring (Tf) uptake increased with
more nucleation – but its extent is likely limited by receptor recycling.
(**B**) Overexpression (0, 1 or 2µg) of myc-Epsin1 induces an increase
of σ2-EGFP (AP2) density at 2µg, which, in contrast to FCHo1/2, is
due to an slowdown of CCP dynamics (see arrows) and results in an
inhibition of Tf uptake. (**C**) In HeLa cells transfected with 0, 0.5, or
1µg of untagged-FCHo2 for 2×10^5 cells, the number of dynamic
CCPs increased proportionally to the levels of untagged-FCHo2
overexpression. By contrast, the number of larger structures (also
called 'clathrin-coated plaques' (S23)) decreased proportionally with
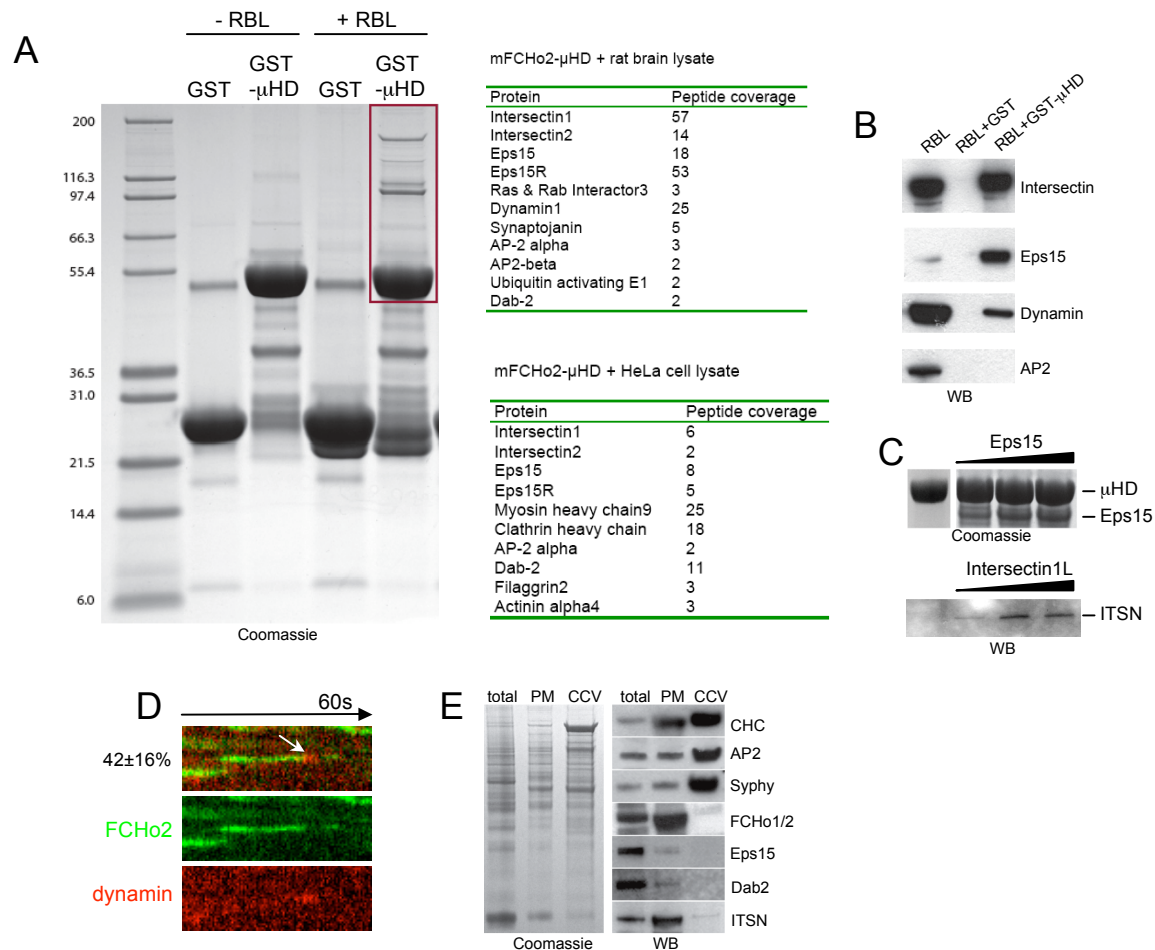the levels of untagged-FCHo2 overexpression (arrows). Scale bar,
5µm.

A

- RBL   + RBL

GST   GST-μHD   GST   GST-μHD

200
116.3
97.4
66.3
55.4
36.5
31.0
21.5
14.4
6.0

Coomassie

mFCHo2-μHD + rat brain lysate

Protein	Peptide coverage
Intersectin1	57
Intersectin2	14
Eps15	18
Eps15R	53
Ras & Rab Interactor3	3
Dynamin1	25
Synaptojanin	5
AP-2 alpha	3
AP2-beta	2
Ubiquitin activating E1	2
Dab-2	2

mFCHo2-μHD + HeLa cell lysate

Protein	Peptide coverage
Intersectin1	6
Intersectin2	2
Eps15	8
Eps15R	5
Myosin heavy chain9	25
Clathrin heavy chain	18
AP-2 alpha	2
Dab-2	11
Filaggrin2	3
Actinin alpha4	3

B

RBL   RBL+GST   RBL+GST-μHD

Intersectin
Eps15
Dynamin
AP2

WB

C

Eps15

— μHD
— Eps15

Coomassie

Intersectin1L

— ITSN

WB

D

60s

42±16%

FCHo2

dynamin

E

total PM CCV   total PM CCV

CHC
AP2
Syphy
FCHo1/2
Eps15
Dab2
ITSN

Coomassie   WB

fig. S6 Supplement for Fig. 2A-D (**A**) Pull downs were conducted with GST-FCHo2 μHD (525-809) fusion protein bound to GSH-sepharose beads. Beads were incubated with rat brain lysate (RBL) for 1 hour, pelleted, washed three times, and run on SDS-PAGE gels. Bands were identified by mass spectrometry (LC-MS-MS). The area highlighted in red corresponds to the pull down shown in Figure 2A. The tables show a more complete list of protein interactions and the peptide coverage from GST-FCHo2 μHD pull downs out of rat brain and HeLa cell lysates. The presence of dynamin is potentially indirect as it binds intersectin with high affinity (S24). (**B**) Western blots of the GST-FCHo2 μHD pull down lysates. Total cell lysate (RBL), RBL+GST, and GST-μHD + RBL were blotted for intersectin1, eps15, dynamin, and AP2-α adaptin subunit. Intersectin and Eps15 displayed enrichment in GST-μHD pull downs, whereas dynamin was de-enriched and AP2-α was absent. (**C**) The interactions between the μHD and eps15 and intersectin are direct. Recombinant eps15 (aa530-791) (0.1, 0.5 and 1mg/ml) and full-length intersectin1L (ITSN) (5, 10 and 20 μg) were titrated into GST-μHD sample on beads in separate experiments, centrifuged and washed. Samples were visualized by Coomassie staining (Eps15) or Western-blotting (ITSN). (**D**) Kymograph of a representative CCP (scoring) labelled with EGFP-FCHo2 (FCHo2) and mCherry-dynamin2 (dynamin). Note the appearance of dynamin after FCHo2 signal diminished rather like the appearance of the yeast Abp1 after the intensity of Syp1p decrease (S16, S21). (**E**) same data than Fig. 2D but including Coomassie loading controls.
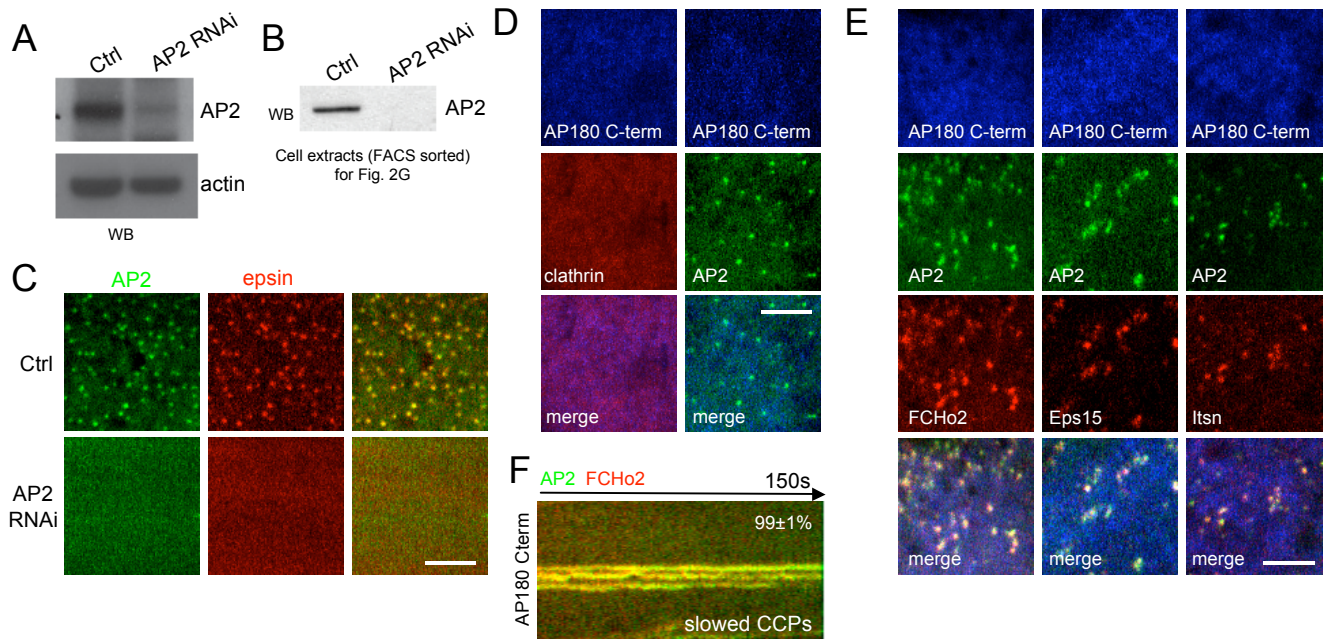
Fig. S7 Supplement for Fig 2F-G (**A**) Down-regulation of AP2 by μ2 RNAi in cells used for live-cell imaging, as verified by western-blot using antibody against AP2-α subunit (when μ2 is depleted, the α subunit of AP2 is destabilized and degraded (S25) (**B**) Down-regulation of AP2 by μ2 RNAi in HeLa cells used for the GST-μHD pull downs in FACS-sorted Hela extracts (see Methods) used in Fig. 2G, as verified by Western-blot using antibody against AP2-α subunit. (**C**) Upon AP2 depletion by μ2 RNAi, both σ2-EGFP (AP2) and Epsin1-RFP (epsin) were cytosolic. (**D**) Overexpression of BFP-AP180 C-terminus (AP180 C-term) abrogated RFP-LCA (clathrin) recruitment to the plasma membrane but not σ2-EGFP (AP2). (**E**) Overexpression of BFP-AP180 C-terminus (AP180 C-term) did not abrogate plasma membrane recruitment of RFP-FCHo2 (FCHo2), RFP-eps15 (Eps15) and RFP-intersectin1L (Itsn). FCHo2, eps15, and intersectin remained colocalized with σ2-EGFP (AP2). (**F**) RFP-FCHo2 (FCHo2) and σ2-EGFP (AP2) spots had slowed dynamics ('slowed CCPs') in BFP-AP180 C-terminus expressing cells, as expected (attributable to the absence of clathrin at plasma membrane puncta). The displayed kymograph was representative (percentage). Scale bars, 5μm.
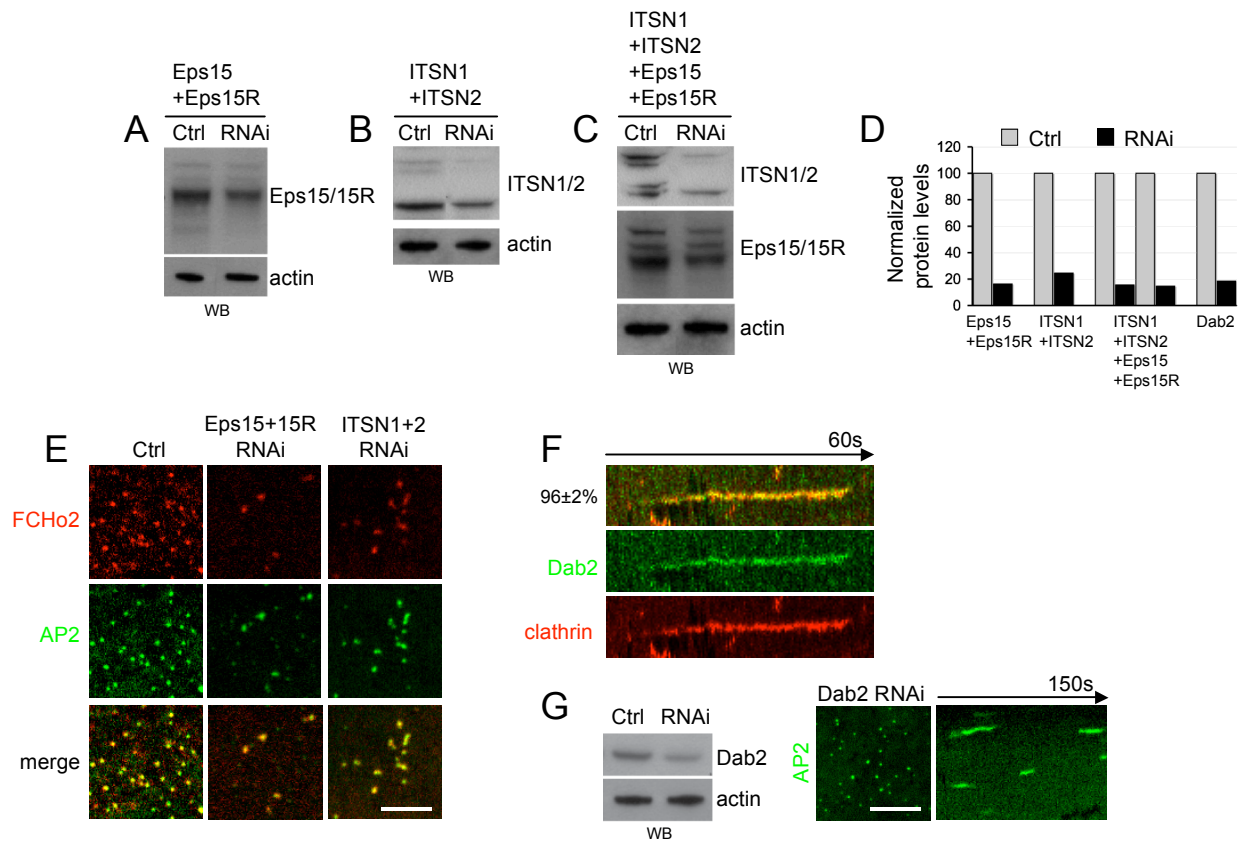
Fig. S8 Supplement for Fig 2H (**A**) Down-regulation of eps15+eps15R by double RNAi in σ2-EGFP expressing cells used for live-cell imaging in E, as verified by Western-blot. (**B**) Down-regulation of intersectin1 + 2 by double RNAi in σ2-EGFP expressing cells used for live-cell imaging in E, as verified by Western-blot. (**C**) Down-regulation of Eps15+Eps15R +Intersectin 1 + 2 by quadruple RNAi in σ2-EGFP cells used for live-cell imaging in Fig. 2G, as verified by Western-blot. (**D**) The incomplete knockdown in RNAi-treated cell cultures used in A, B, C and G was due to a transfection efficiency of ~20%, as judged by the expression of RFP-tagged respective proteins which explains why depletion of these proteins was not complete by Western Blot analysis of the whole population. Quantification of the Western-blot bands of the gels presented in A, B, C and G, (background-corrected, actin-level normalized and corrected for 20% transfection) predicted between 75 to 85 % decrease in proteins levels in transfected cells. (**E**) The number of RFP-FCHo2 (FCHo2) and σ2-EGFP (AP2) puncta decreased under both eps15 + eps15R (Eps15+15R) and itsn1 + itsn2 (ITSN1+2) double RNAi. (**F**) Kymograph of a representative CCP labelled with EGFP-Dab2 (Dab2) and RFP-LCa (clathrin). Dab2 was recruited early to CCP but not before clathrin. The displayed kymograph was representative (percentage). (**G**) Down-regulation of Dab2 by RNAi as verified by western-blot. BSC1 σ2-EGFP (AP2) cells transfected with Dab2 RNAi displayed normal nucleation rate of AP2 (5.8±0.8 number of new clathrin-coated pits/10^4 μm²/second *versus* 6.8±1.1 for control, *p*<0.01).
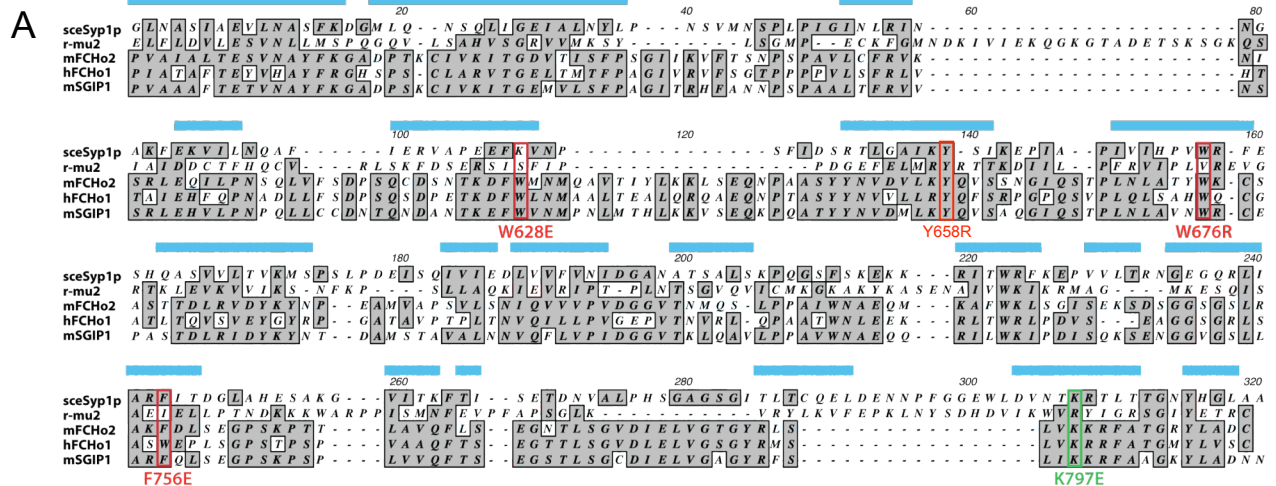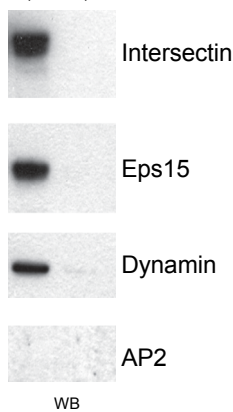
fig. S9 Supplement for Fig. 2 I-J (**A**) Structure-based alignment of the recently solved µHD of yeast Syp1p (3G9H) and rat µ2 (1I32) compared with µHDs of FCHo2 (Riken AK142282), FCHo1 (IMAGE 5757146), and SGIP1 (AAH17596). Mutated residues that did not express in *E.coli.* are shown in red. K797E (green) was used in Fig. 2G. β-sheets are denoted by blue bars. (**B**) Pull-downs were conducted with GST-FCHo2 µHD (525-809, K797E) fusion protein bound to GSH-sepharose beads. Beads were incubated with rat brain lysate (RBL) for 1hour, pelleted, washed three times, and run on SDS-PAGE gels. GST-µHD + RBL and GST-µHD Y555A+K797E + RBL were blotted for Intersectin1, Eps15, Dynamin, and AP2-α subunit. All were absent in the pull-down performed with the mutant. Although this pull down was done with the double mutant Y555A+K797E, Y555A alone mutants display no phenotypes alone by pull down nor *in vivo* (*not shown*), thus the phenotype here was attributed to mutation K797E.
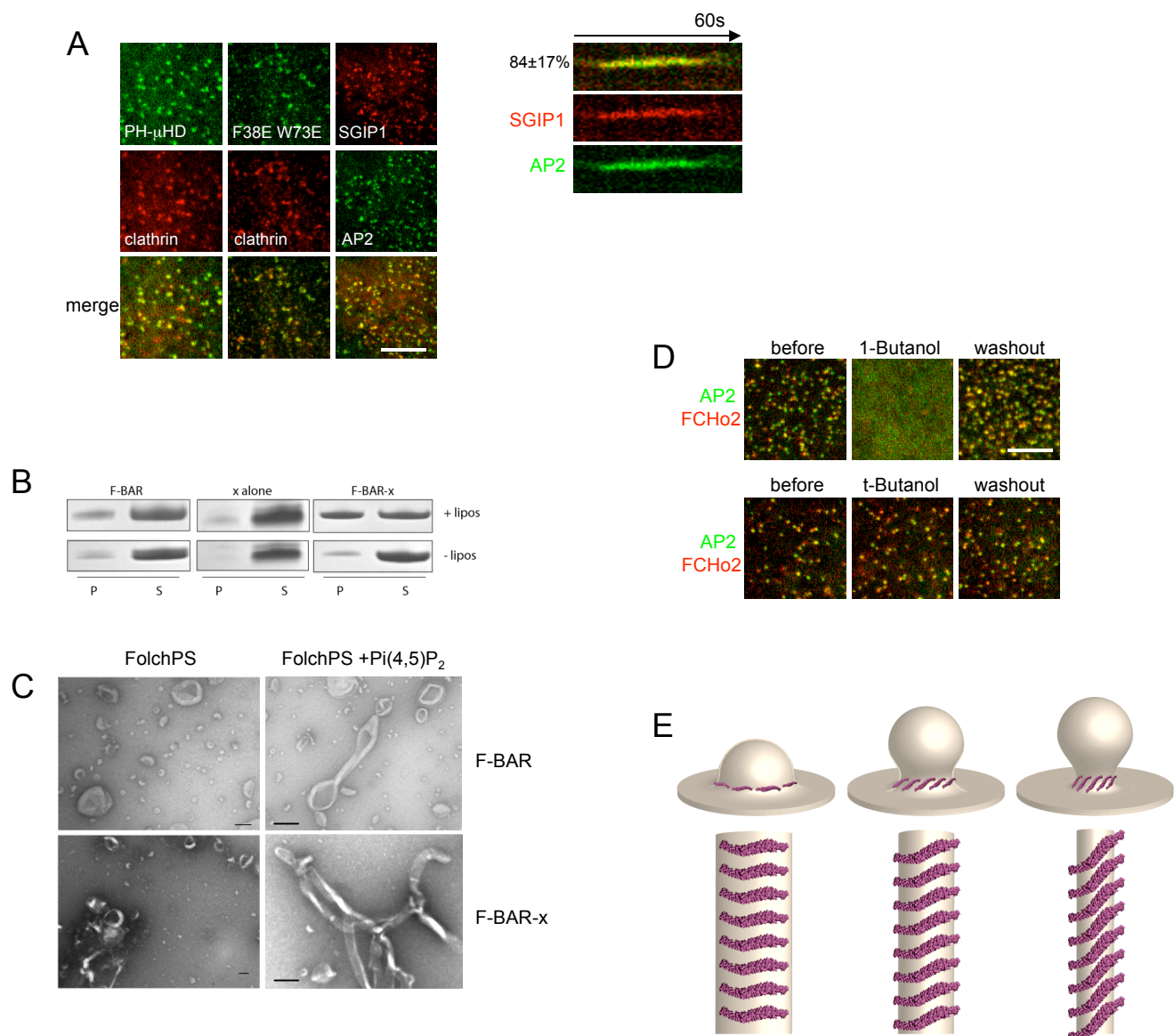
fig. S10 Supplement for Fig. 3A-C (**A**) A chimera EGFP-PH-μHD (PH-μHD), an FCHo2 which cannot dimerize EGFP-FCHo2 (F38E+W73E), and RFP-SGIP1 were all targeted to CCP in normal (non-RNAi treated) cells. SGIP1 was an early component in CCP formation but was not detected before AP2, as shown on the kymograph of a representative CCP labelled with RFP-SGIP1 (SGIP1) and σ2-EGFP (AP2). The displayed kymograph was representative (percentage). (**B**) The F-BAR and extended (x) domains acted synergistically to enhance lipid membrane binding. Lipid-protein co-sedimentation assays of F-BAR-x (1-327), F-BAR (1-262), and x (263-430) proteins with 0.5mg/mL liposomes (see Methods for composition). All proteins were used at 15μM concentration. Samples were incubated, centrifuged, and separated into pellet (P) and supernatant (S) fractions, and run out on SDS-PAGE gel electrophoresis. (**C**) $Pi(4,5)P_2$ stimulated membrane tubulation by the FCHo2 F-BAR-x module. 5μM of FCHo2 F-BAR (1-262) or FCHo2 F-BAR-x (1-327) protein were incubated with Avanti Folch liposomes spiked with either 20% phosphatidylserine (FolchPS) or FolchPS + 5% $Pi(4,5)P_2$ (Folch+$Pi(4,5)P_2$), and evaluated by EM. No tubulation was observed by either F-BAR or F-BAR-x protein on Folch+PS liposomes. Moderate tubulation was seen by F-BAR protein on FolchPS +$Pi(4,5)P_2$ liposomes, and tubules were broad in diameter (70-130nm). The F-BAR-x module produced a higher degree of membrane tubulation of FolchPS+$Pi(4,5)P_2$ liposomes. Scale bars, 200 nm (**D**) The acute decrease of cellular $Pi(4,5)P_2$ by the addition of 2% of the primary alcohol 1-butanol (S13) induced reversible loss of FCHo2 plasma membrane localization. EGFP-FCHo2 (FCHo2) and RFP-LCa (clathrin), which colocalize in the cell before treatment, became cytosolic within 1 minute following the addition of 2% 1-butanol, as observed by live-cell imaging. Following washout of 1-butanol, FCHo2 and clathrin rapidly relocalized to the plasma membrane. During 1-butanol washout, nucleation rate were transiently higher, as reported earlier (S13). As expected, 2% of the tertiary alcohol t-butanol had no effect (bottom panel). Scale bar, 5 μm. (**E**) A model indicating how the F-BAR dimer can support both moderate and extreme positive membrane curvature. When the F-BAR dimer orients perpendicular to the long axis of a membrane tubule, only moderate curvature is generated since the F-BAR dimer is only shallowly curved. If the F-BAR dimers are shifted to an oblique angle, however, high curvature is generated (see Supplementary Movie S2). This may explain how FCHo2 can localize to relatively flat regions of the plasma membrane, accumulate, and create the initial dimple of the nascent CCP.
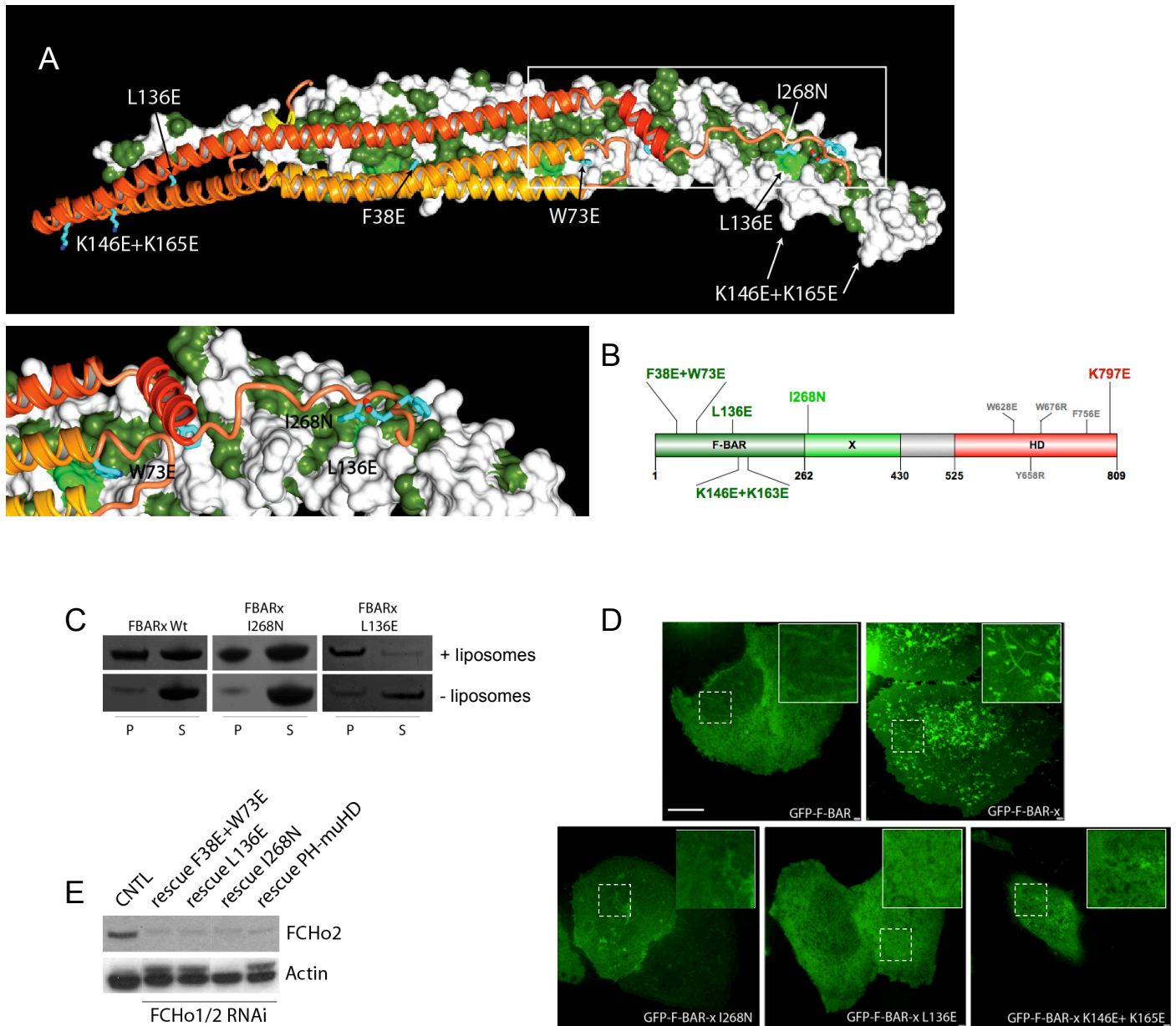
fig. S11 Supplement for Fig. 3D-E (A) Structure-based mutations of the F-BAR and extended (x) domains which affect CCP formation and transferrin uptake (refer to Fig 4D). The lipid binding mutants (K146E+K165E) are located on the concave face of the F-BAR dimer. The dimer interface mutants (F38E+W73E) are buried within the dimer core. I268N lies on the beginning of the extended domain and faces inward into the conserved hydrophobic pocket along the F-BAR 'wing'. This mutation is derived from the I282N mutation is mouse protein MAYP which generates a macrophage-associated autoimmune disease (S26). L136E is across from I268N and interacts directly in the hydrophobic pocket. (B) Structure-based mutations scheme on FCHo2. (C) F-BAR-x mutants that lose tubulation ability still bound to lipid membrane *in vitro*. Lipid protein co-sedimentation assays with mutant F-BAR-x protein and Avanti Folch liposomes (+20% PS and 5% Pi(4,5)P$_2$). Protein and liposomes were incubated, centrifuged, and the pellet (P) and supernatant (S) were separated and run on SDS-PAGE gels. Mutant proteins I268N and L136E cosedimented with liposomes in amounts comparable to WT protein. (D) An *in vivo* tubulation assay to assess mutations that affect membrane sculpting. HeLa cells expressing EGFP-FCHo2 F-BAR (1-272) or F-BAR-x (1-327). The F-BAR domain alone generated few plasma membrane tubules in HeLa cells when over-expressed, but expressing of F-BAR-x lead to membrane tubulation (see inset). Mutants attenuate membrane tubulation and lead to a diffuse plasma membrane signal (see insets). Scale bar, 20 μm (E) FCHo1/2-depleted BSC1 cells expressing RNAi-resistant mutants FCHo2 FL (see chart Fig. 3D). Western blots against FCHo2 demonstrate ~80% knockdown of endogenous FCHo2.
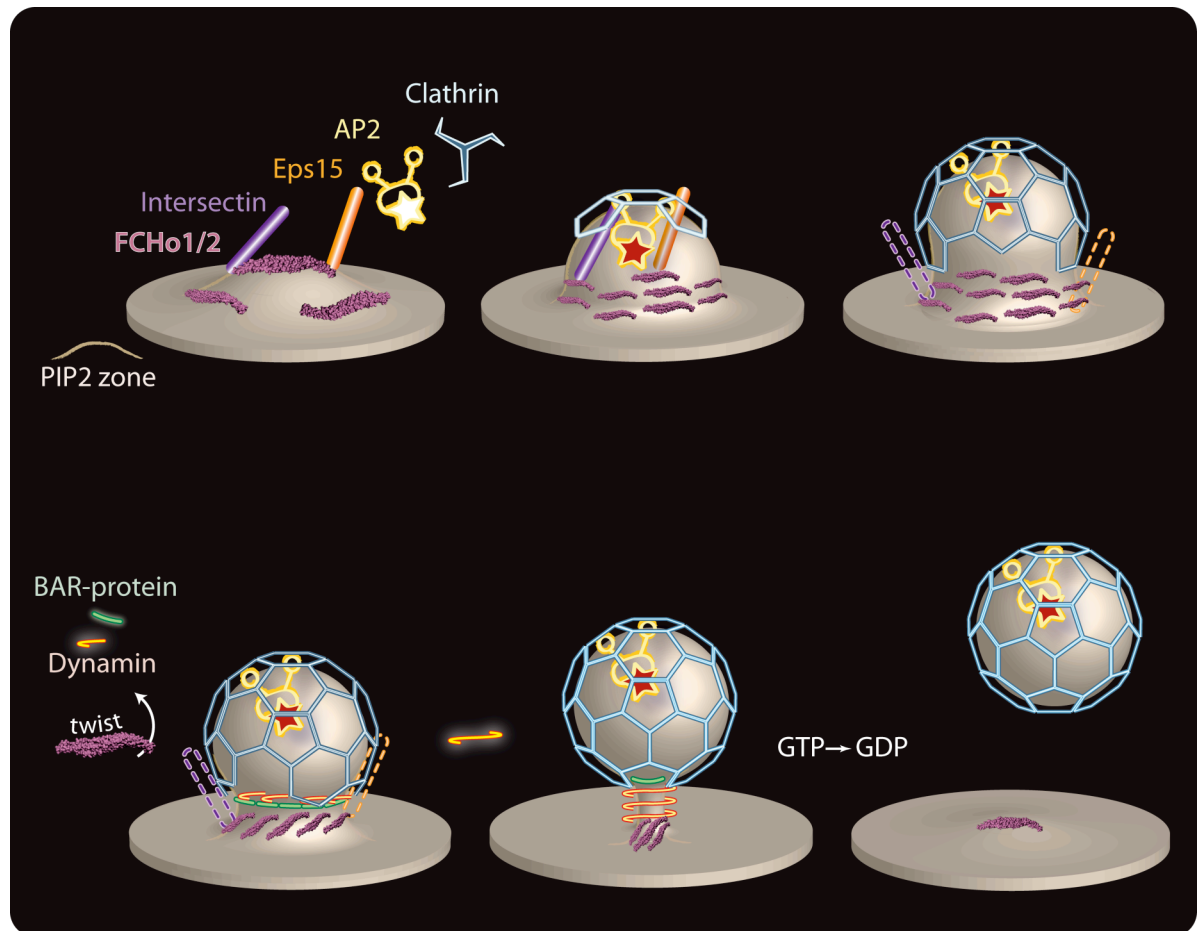
fig. S12 A model for FCHo1/2 proteins as nucleators of CCP formation. FCHo proteins bind to the plasma membrane at sites where CCPs will form. They recruit the early CCP proteins eps15 and intersectin, which function to cluster FCHo proteins into puncta and generate the initial curvature. As FCHo protetins and Eps15 (S27) accumulate at the rim of nascent CCP, more extreme curvatures are generated by FCHo proteins as they accumulate and change their angle on the membrane. Eps15 and intersectin recruit AP2, which can subsequently engage clathrin and additional accessory factors necessary for maturation of vesicle formation and budding.

Supplementary movies and legends:

Supplementary Movie S1: BSC1 σ2-EGFP cells imaged for 150 frames at 2s interval using a spinning-disk confocal. Control (left panel) or transfected (2μg of untagged FCHo2 plasmid, right panel). The movie was accelerated 10 times. Please note the increased density of CCP with FCHo2 overexpression.

Supplementary Movie S2: Simulation of membrane bending by multiple F-BAR dimer modules. The FCHo2 F-BAR module was based on the crystal structure (pdb: 2V0o). The F-BARs are initially recruited to flat membrane, and as they accumulate, they generate membrane curvature and shift to support a more extreme membrane curvature by reorienting at an oblique angle relative to the tubule axis.

Authors contributions:

W.M.H. performed lipid co-sedimentation, tubulation assays, CCV purification and imaging, E.B. performed live-cell imaging, ligand uptake assays, and quantification of CCP dynamics, M.M. performed pull-down experiments and in vitro binding, E.E. performed cryoimmuno electron microscopy and in vitro binding, Y.V. prepared hippocampal neurons, R.M. provided guidance and reagents and H.M.M. supervised the project. H.M.M., E.B., and W.M.H. wrote the paper with input from all the other authors.

Supporting References:

S1.   Shaner, N.C., et al., *Improving the photostability of bright monomeric orange and red fluorescent proteins.* Nat Methods, 2008. 5(6): p. 545-51.
S2.   Ellis, M.V., et al., *Catalytic domain of phosphoinositide-specific phospholipase C (PLC). Mutational analysis of residues within the active site and hydrophobic ridge of plcdelta1.* J Biol Chem, 1998. 273(19): p. 11650-9.
S3.   Hussain, N.K., et al., *Endocytic protein intersectin-l regulates actin assembly via Cdc42 and N-WASP.* Nat Cell Biol, 2001. 3(10): p. 927-32.
S4.   Benmerah, A., et al., *The tyrosine kinase substrate eps15 is constitutively associated with the plasma membrane adaptor AP-2.* J Cell Biol, 1995. 131(6 Pt 2): p. 1831-8.
S5.   Fazioli, F., et al., *eps15, a novel tyrosine kinase substrate, exhibits transforming activity.* Mol Cell Biol, 1993. 13(9): p. 5814-28.
S6.   Fujita, H., et al., *Rapostlin is a novel effector of Rnd2 GTPase inducing neurite branching.* J Biol Chem, 2002. 277(47): p. 45428-34.
S7.   Granseth, B., et al., *Clathrin-mediated endocytosis is the dominant mechanism of vesicle retrieval at hippocampal synapses.* Neuron, 2006. 51(6): p. 773-86.

S8.   Morris, S.M. and J.A. Cooper, *Disabled-2 colocalizes with the LDLR in clathrin-coated pits and interacts with AP-2.* Traffic, 2001. 2(2): p. 111-23.

S9.   Ford, M.G., et al., *Curvature of clathrin-coated pits driven by epsin.* Nature, 2002. 419(6905): p. 361-6.

S10.   Ford, M.G., et al., *Simultaneous binding of PtdIns(4,5)P2 and clathrin by AP180 in the nucleation of clathrin lattices on membranes.* Science, 2001. 291(5506): p. 1051-5.

S11.   Girard, M., et al., *Isolation of clathrin-coated vesicles by differential and density gradient centrifugation.* Curr Protoc Cell Biol, 2005. Chapter 3: p. Unit 3 13.

S12.   Ehrlich, M., et al., *Endocytosis by random initiation and stabilization of clathrin-coated pits.* Cell, 2004. 118(5): p. 591-605.

S13.   Boucrot, E., et al., *Role of lipids and actin in the formation of clathrin-coated pits.* Exp Cell Res, 2006. 312(20): p. 4036-48.

S14.   Sigismund, S., et al., *Clathrin-independent endocytosis of ubiquitinated cargos.* Proc Natl Acad Sci U S A, 2005. 102(8): p. 2760-5.

S15.   Reider, A., et al., *Syp1 is a conserved endocytic adaptor that contains domains involved in cargo selection and membrane tubulation.* Embo J, 2009. 28(20): p. 3103-16.

S16.   Stimpson, H.E., et al., *Early-Arriving Syp1p and Ede1p Function in Endocytic Site Placement and Formation in Budding Yeast.* Mol Biol Cell, 2009.

S17.   Diril, M.K., et al., *Stonin 2 is an AP-2-dependent endocytic sorting adaptor for synaptotagmin internalization and recycling.* Dev Cell, 2006. 10(2): p. 233-44.

S18.   Roux, A., et al., *Membrane curvature controls dynamin polymerization.* Proc Natl Acad Sci U S A, 2010. 107(9): p. 4141-6.

S19.   Collins, B.M., et al., *Molecular architecture and functional model of the endocytic AP2 complex.* Cell, 2002. 109(4): p. 523-35.

S20.   Uezu, A., et al., *SGIP1alpha is an endocytic protein that directly interacts with phospholipids and Eps15.* J Biol Chem, 2007. 282(36): p. 26481-9.

S21.   Boettner, D.R., et al., *The F-BAR protein Syp1 negatively regulates WASp-Arp2/3 complex activity during endocytic patch formation.* Curr Biol, 2009. 19(23): p. 1979-87.

S22.   Martina, J.A., et al., *Stonin 2: an adaptor-like protein that interacts with components of the endocytic machinery.* J Cell Biol, 2001. 153(5): p. 1111-20.

S23.   Saffarian, S., E. Cocucci, and T. Kirchhausen, *Distinct dynamics of endocytic clathrin-coated pits and coated plaques.* PLoS Biol, 2009. 7(9): p. e1000191.

S24.   Gout, I., et al., *The GTPase dynamin binds to and is activated by a subset of SH3 domains.* Cell, 1993. 75(1): p. 25-36.

S25.   Motley, A., et al., *Clathrin-mediated endocytosis in AP-2-depleted cells.* J Cell Biol, 2003. 162(5): p. 909-18.

S26.   Grosse, J., et al., *Mutation of mouse Mayp/Pstpip2 causes a macrophage autoinflammatory disease.* Blood, 2006. 107(8): p. 3350-8.

S27.   Tebar, F., et al., *Eps15 is a component of clathrin-coated pits and vesicles and is located at the rim of coated pits.* J Biol Chem, 1996. 271(46): p. 28727-30.